Explosive vent sites on mercury: Commonplace multiple eruptions and their implications

Icarus 365 (2021) 114510

Contents lists available at ScienceDirect

Icarus

journal homepage: www.elsevier.com/locate/icarus

Explosive vent sites on mercury: Commonplace multiple eruptions and their implications

D.L. Pegg [a,*], D.A. Rothery [a], M.R. Balme [a], S.J. Conway [b]

[a] The Open University, Milton Keynes MK7 6AA, UK
[b] CNRS, Laboratoire de Planétologie et Géodynamique UMR 6112, Université de Nantes, France

ARTICLE INFO

Keywords:
Mercury
Volcano
Pyroclastic
Compound vents
Explosive volcanism

ABSTRACT

Explosive volcanic vents are widespread on Mercury. Compound volcanic vents comprise multiple individual vents, and probably formed through multiple events. We demonstrate that ~70% of the volcanic vent sites on Mercury that have been imaged with sufficient resolution to resolve their internal features are compound vents that have probably undergone multiple eruptions. Interior characteristics of compound vents, such as cross-cutting relationships, contrasts in small scale impact cratering, and other textural detail, as well as the asymmetry of surrounding faculae, suggest that activity occurred over a prolonged but so far unquantified period of time. We use multiple case studies to highlight the migration of eruption centres at these sites. At the Nathair Facula vent, small-scale interior pits suggest the location of the most recent activity.

1. Introduction

Explosive volcanism has occurred on Mercury, Venus, Earth, the Moon, Mars, Io and possibly Titan (Greeley and Spudis, 1981; Wilson, 2009; Wilson and Head, 2017; Wilson and Head, 1983; Wood and Radebaugh, 2020). On Mercury, the products of explosive volcanism are manifest as relatively red, high-albedo surficial deposits (compared to the global mean) in enhanced-colour images from Mariner 10 (Rava and Hapke, 1987) and MErcury Surface, Space ENvironment, GEochemistry, and Ranging (MESSENGER)'s Mercury Dual Imaging System (MDIS); (Head et al., 2009; Kerber et al., 2009). These high-albedo red spots are now known by the descriptor term *facula* (plural *faculae*). These faculae are 10 s to 100 s km in diameter, and they have been interpreted as ballistically-dispersed pyroclastic products of explosive eruptions mantling (draped over) the surrounding terrain, subduing, but rarely entirely obscuring, underlying textures (Kerber et al., 2009). They usually contain a central 'pit' (up to several km deep and up to 10s of km wide) that is the likely site of the source (vent) from which the pyroclastic materials were erupted. Not all pits have a discernible facula, and conversely some faculae lack pits and may have a different origin (Thomas et al., 2014a).

Some of the vent sites probably represent the latest volcanic activity on Mercury. With faculae forming as recently as the early Kuiperian (Thomas et al., 2014b; Jozwiak et al., 2018) and hence no older than 280 Ma (Banks et al., 2016), much more recently than large-scale effusive volcanism which ended 3.5 at about Ga (Byrne et al., 2016). Unlike impact craters, the pits marking vent sites are usually non-circular (often scallop-edged) and lack a raised rim. To avoid confusion with the raised rim of an impact crater, the edge of a pit is conveniently referred to by the term 'brink' in preference to 'rim' (Rothery et al., 2014). The vent sites do not sit within prominent constructional volcanic edifices. Brož et al. (2018) attribute this to the low gravity and lack of atmosphere leading to the wide dispersal of pyroclastic materials resulting in flank slopes of less than 2.8°.

Explosive vent sites on Mercury are important to study as they provide evidence of the volatile rich nature of Mercury's crust and interior (Kerber et al., 2009; Weider et al., 2016), as well as providing insights into the planet's thermal and tectonic history. Their activity continued more recently than has been demonstrated for effusive volcanism (Byrne et al., 2018; Byrne et al., 2016). This is especially interesting as the majority of Mercury's crust is under compression due to global contraction which should generally inhibit the ascent of magma (Klimczak et al., 2015) which should inhibit the volcanism (Byrne et al., 2018).

Compound volcanoes are those that have multiple overlapping vents and edifices (Davidson and De Silva, 2000; Jackson and Bates, 1997). Overlapping and crosscutting features show, according to the principle of superposition (Lyell, 1853), that they form by a succession of events.

* Corresponding author.
E-mail address: david.l.pegg@open.ac.uk (D.L. Pegg).

https://doi.org/10.1016/j.icarus.2021.114510
Received 19 August 2020; Received in revised form 22 April 2021; Accepted 26 April 2021
Available online 29 April 2021

A terrestrial example of a compound volcanic vent is Volcán Aucanquilcha in Chile; this comprises 20 individual vents, some within overlapping craters, ranging in age from 11 Ma to <1 Ma (Klemetti and Grunder, 2008). Rothery et al. (2014) used the term 'compound volcano' when describing the vent complex inside Agwo Facula, for which Thomas et al. (2014b) coined the term 'compound vent' (Fig. 1). The vent complex consists of nine internal depressions (vents), some separated only by thin walls (septa). They regarded these depressions as individual vents, within an overall compound vent site. Crosscutting relationships between the individual vents and differences in surface roughness between them suggest that eruptions occurred over a prolonged period.

Until now, only limited studies of the eruptive history of vent sites on Mercury have been undertaken, other than to give an approximate maximum age of those occurring within impact craters (Goudge et al., 2014; Thomas et al., 2014a; Jozwiak et al., 2018). We present here a study of all identified volcanic vent sites on Mercury, assess the available image data, and determine what proportion are compound. We note relevant small features and possible migration within vents, we discuss the histories inside a selection of individual vent sites, we draw attention to some asymmetric faculae, and we discuss the implications for Mercury's volcanic history.

2. Material and methods

To investigate all the known volcanic vent sites on the planet and identify the proportion that are compound, we conducted a review of the existing lists of vents and faculae (Kerber et al., 2011; Goudge et al., 2014; Thomas et al., 2014a; Jozwiak et al., 2018). We added 27 further vent sites that we identified during our own study of Mercury, and re-examined areas previously identified as "pitted ground" (Thomas et al., 2014c) to see whether higher resolution image data collected subsequently would reveal volcanic vents not identified in previous data.

2.1. Image data

To inspect each known vent site and/or facula, we used the highest resolution (<180 m/pixel) narrow-angle camera and wide-angle camera images captured by MESSENGER's MDIS instrument (Hawkins et al., 2007) and archived in the NASA Planetary Data System. We projected the image data using USGS ISIS3 software. To study each vent location, we re-projected the images using a sinusoidal projection centred at the midpoint of the vent/facula and displayed images using geographical information system (GIS) software. We used the 665 m / pixel enhanced colour mosaic (Denevi et al., 2016) to examine faculae, though not all vent sites show faculae and not all faculae contain vents (Jozwiak et al., 2018). We visually examined each location to verify vent sites by identifying depressions lacking raised rims. We excluded hollows through their relatively blue reflectance (Blewett et al., 2011) in the enhanced colour basemap, highly localised albedo (compared to the generally more diffuse anomalies of faculae), generally flat floors, and relatively small (~100 s of meters) size (Blewett et al., 2011). We excluded impact craters by their raised rims and ejecta patterns. We defined a vent site as "a depression bounded by a single brink spatially separated from other sites".

We do not consider faculae containing only pitted ground to be vent sites; pitted ground has rough floors without a large scale (>1 km) pit, and perhaps forms when lava flows over volatile-rich materials causing local volatile release through the lava, thus disrupting the lava surface and creating the albedo feature but without an explosive event capable of excavating a substantial pit (Fig. 2) (Thomas et al., 2014c). This paper focuses on vent sites, and faculae without clear vent sites are excluded from the rest of the study.

We made a trial of digital elevation models (DEMs) of vent site interiors using AMES Stereo Pipeline (Broxton and Edwards, 2008). However, we found that the lack of good image pairs at sufficient resolution to identify the detailed internal morphology of vent sites resulted in less information being conveyed in these DEMs than by individual images, or by images with much different illumination angles that clearly highlight morphology but are unsuitable for DEM creation. The time needed to produce DEMs for all vent sites and the lack of any benefit in the majority cases means that the bulk of this study relies on photogeological interpretation (e.g., Allum, 2013).

2.2. Identification of compound vent sites

We applied three-level semi-quantitative confidences to our classification of the vent sites (as compound or otherwise), based on our assessment of the available images. If the image quality was insufficient to distinguish between impact craters and vents or to identify internal structures or features within the vent sites, we recorded the vent sites as "unclassifiable". This usually corresponds to vents imaged only once, often with a solar incidence angle >80° (where shadows may obscure features) or close to 0° (where topographic features are no longer clear), or imaged at a resolution that is insufficient to make out the interior of vents (this is dependent on the size of the vent). Conversely, vent sites with "good image quality" had illumination adequate to show the vent interiors clearly, and perhaps several images with various incidence or emission angles. In between these extremes, "reasonable image quality" vent sites often required inspection of multiple images to identify breaks in slope or to reveal other morphology clearly.

At each vent site we searched for morphological features, and then decided whether each vent site is compound. We used the one or more of

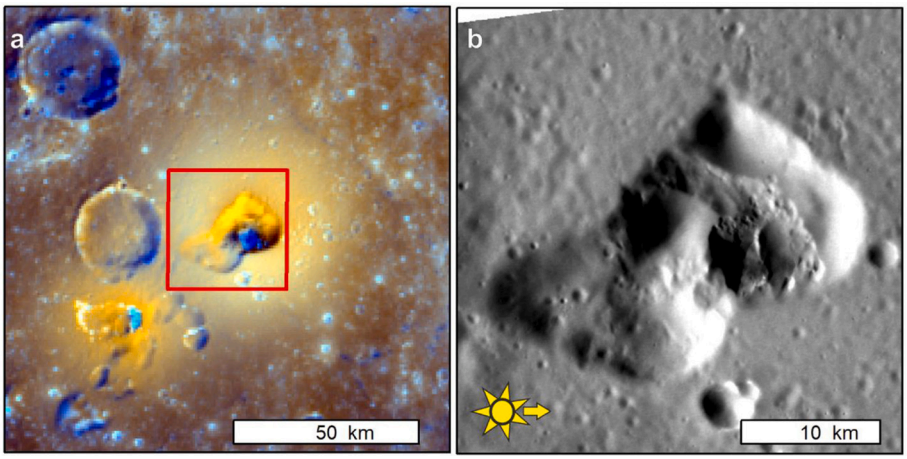

Fig. 1. The compound vent at Agwo Facula a. Enhanced colour image from global enhanced colour mosaic (Denevi et al., 2016). Red box is the outline of 1b. b. The detailed internal structure revealed in a MESSENGER image EN1060657198M (55 m / pixel). Images centred at 146.1° E, 22.4° N in a sinusoidal projection. North towards the top of all images. Image credit: NASA/ Johns Hopkins University Applied Physics Laboratory/Carnegie Institution of Washington. (For interpretation of the references to colour in this figure legend, the reader is referred to the web version of this article.)

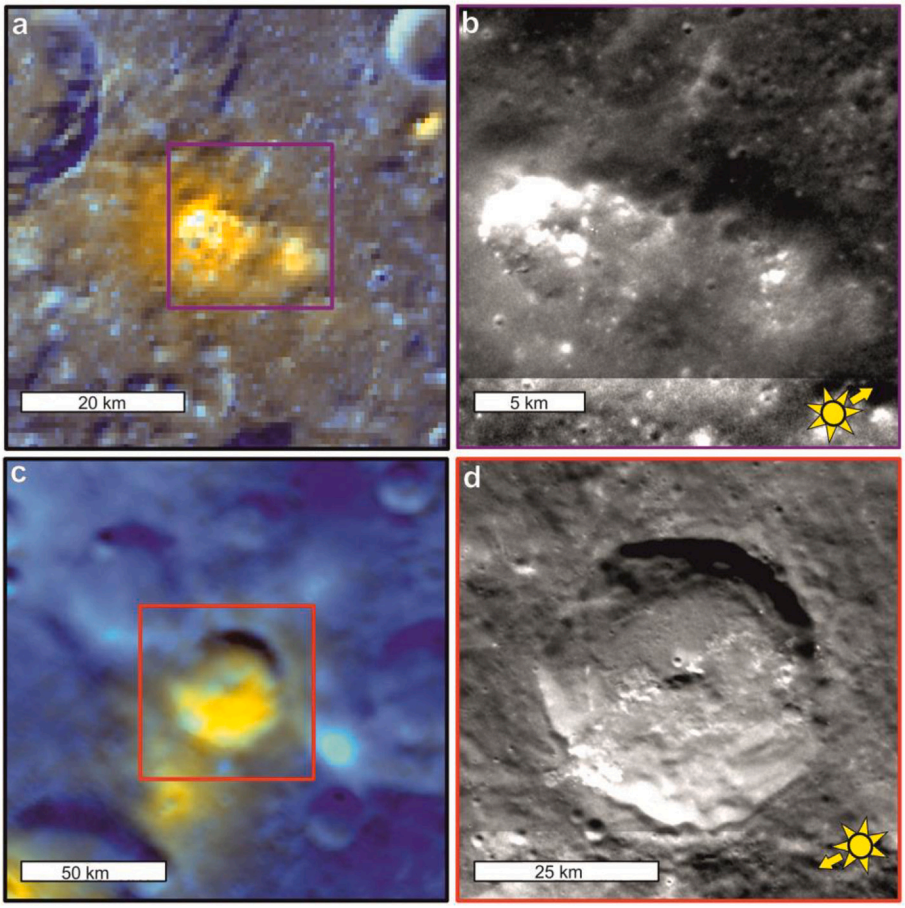

Fig. 2. Examples of features not classified as a vent a. Enhanced colour basemap (Denevi et al., 2016) showing faculae known only on poorly resolved image data. Box shows the extent of b. Image centred at 141.4°E 38.3°N. b. Image of EN0233460948M poorly illuminated depression (not a clear vent) hosting hollows, 33 m/pixel. c. Enhanced colour basemap (Denevi et al., 2016) showing a facula with no resolved vent (likely pitted ground). Box shows the extent of d. Image centred at −27.8°E − 51.5°N d. Image EN1035383880M showing the high-resolution image of the facula without a vent, 118 m/pixel.

the following morphological characteristics within vents used to recognise a compound volcanic vent:

- Presence of internal structures such as septa that subdivide vents (Fig. 3a)
- Immediately adjacent vents where parts of the brinks touch (Fig. 3b)
- Larger vents that contain smaller vents (Fig. 3d)

Septa are internal walls subdividing a vent site. Where multiple vents directly touch (for example with only a thin septum), we consider them to be part of the same compound vent site. When there is intervening flat ground, we log them as separate vent sites even if distributed around the same structure (such as around a crater's central peak). Both these structures are spatial evidence for multiple eruptions because they demonstrate discrete eruption sites. When there is a smaller vent inside a larger vent (e.g. Fig. 3d), the smaller vent must postdate the larger vent that hosts it, because the larger vent floor had to exist before the smaller could form, and so these are also compound vent sites evidencing temporal evidence of multiple eruptions.

On Earth, compound volcanoes are identified either by overlapping edifices or by intersecting volcanic craters (Neuendorf et al., 2005). The lack of significant edifices on Mercury makes our definition, based only on the pits corresponding to each vent, more conservative than on Earth. However, it follows the same usage of the term 'compound volcanic vent' as previous work on Mercury (Rothery et al., 2014; Thomas et al., 2014b).

We applied to each vent site the following classification: compound, ambiguous, or not compound. Additionally, we noted those examples where image quality was insufficient to enable classification. We recorded as "ambiguous" those sites that have some form of structure, but do not have clearly defined separate vents (for example where septa are missing or incomplete), or where it was plausible to ascribe internal structures to processes such as mass wasting or fault activity. We took a conservative approach in recording the vent site inside Nathair Facula (commonly referred to as "the north-east Rachmaninoff vent" before the facula received its formal name in 2018) as "ambiguous" due to lack of clear structural division, even though differences in mantling and areas with rough floor texture suggest a multi-stage history. We discuss this example further in Section 3.1. The link to a list of images used to classify vent sites is in the Data Availability section.

Processes that could have modified the inside of vents, other than multiple separate eruptive events or migration of the eruption centre during an eruption, include:

1. Gravity-driven mass wasting (movement of rock debris downslope due to gravity)
2. The asymmetric build-up of erupted materials

Mass wasting is a likely process to occur after the creation of new slopes on Mercury and is known to occur within craters (Brunetti et al., 2015) and at the edges of some vents (Malliband et al., 2019). Likely examples are easily identified on the interior slopes of vents (see the north of Fig. 3e) where mass wasting, sufficient to change the outline of the vent, has occurred. Mass wasting could be a cause of some of the unusual shapes of vent brinks and the alternation of convex and concave planform shapes. However, mass-wasting deposits can be identified on the floor of vents by their positive topographic convex-up lobate form (Brunetti et al., 2015). We do not consider it likely that morphologies created by mass wasting would be similar to the features used to identify compound volcanic vents shaped by volcanic processes.

We consider that the build-up of explosive volcanic ejecta asymmetrically (where volcanic materials accumulate on one section of the

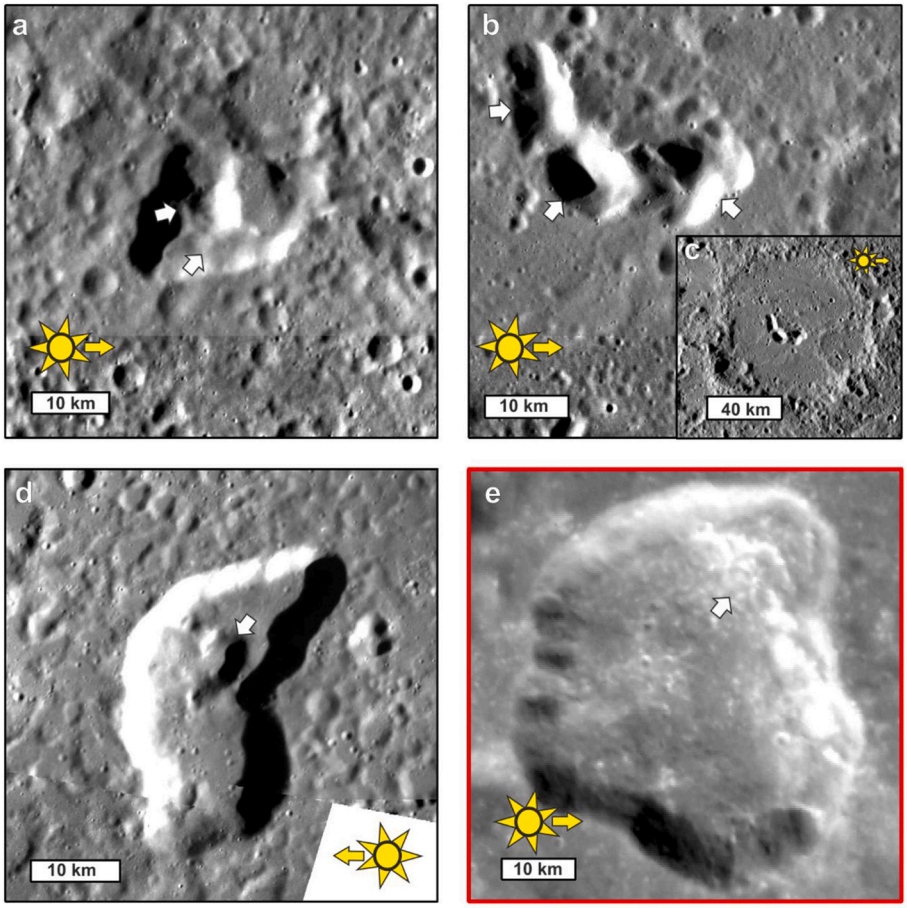

Fig. 3. Examples of vents with morphological features used to distinguish compound and non-compound (red outline) vent sites a. A triangular compound vent subdivided by multiple septa (arrows highlight some of the septa). Image centre: -49.0°E, −27.5°N, image: EN0213201259M b. A compound vent site on a crater floor comprising a set of multiple adjacent volcanic vents. Arrows point to individual vents, Image: EN0250970163. c. context for vents in b, showing vents arcing round the southern edge of an inferred buried central peak, image: EW0220721409G. Image b and c centre: 143.6°E, −5.1°N,. d. A smaller vent (arrowed) in the floor of a larger vent. Image centre: 22.6°E, 32°N image: EN0220030413M e. Large volcanic vent with concave and convex portions along its brink; an example of a kind that we, conservatively, do not classify as compound. The arrow points to the area of mass wasting in the north. Image Centre: 57.3°E, 36.0°N, image: EW0234906641G. North towards the top of all images. Image credits: NASA/ Johns Hopkins University Applied Physics Laboratory/Carnegie Institution of Washington. (For interpretation of the references to colour in this figure legend, the reader is referred to the web version of this article.)

vent/volcano during an eruption) is unlikely to produce morphologies similar to compound volcanic vents because the ejecta is so thinly dispersed that departure from radial symmetry would not affect the within-vent topography (Brož et al., 2018; Thomas et al., 2014b). Asymmetric distribution of ejecta could, however, produce an asymmetric facula (Section 3.2).

Where the image data were sufficient to study the relationships of the internal component vents within a compound volcanic vent site, we looked for crosscutting relationships to infer relative timing. We also reason that smoother surfaces in and around vents are likely to represent older portions of a compound volcanic vent than rougher surfaces nearby, due to mantling by younger volcanic ejecta from nearby vents subduing their textures, or being old enough to have developed a thicker regolith cover (Rothery et al., 2014).

We studied some case studies (Section 3.1) and mapped them out in ArcGIS at a scale of 1:2000 times the pixel size (in metres) of the images (listed in the example figure captions). We interpreted shadows, in some cases switching between multiple illuminations, to divide each compound volcanic vent into individual vents/depressions. We deduced relative timing from crosscutting relationships such as where edges of vents further excavated pre-existing floors (Fig. 3c) or cut through the brinks of other vents showing that those must have formed earlier (Fig. 3b). We visually assessed relative surface roughness and compared this with the crosscutting relationships.

3. Results

We have identified a total of 309 vent sites across the planet. Of these, 109 are imaged with good image quality, 115 have reasonable image quality and 85 are unclassifiable. Of the 309 vent sites, 131 are clearly compound volcanic vents, and 57 are clearly not. The remaining 121 are either ambiguous or unclassifiable (Table 1). Of the 309 vent sites, 87% have an associated facula. We find that the presence of a facula has no relation to whether the vent is compound or not, and that 90% of non-compound vents have a facula (See Data Availability for the link to the list of vents).

Table 1 shows that of the vent sites with good image quality 71% of vents are compound (Fig. 4). Of all vents sites studied 42% of all vent sites are definitely compound, and only 18% are definitely not compound. Excluding all the unclassifiable and ambiguous examples, but including reasonable image quality, 70% of the confidently classified vent sites are compound, and 30% are not (Fig. 4) showing that it is possible to identify compound vents even on sub-optimal images. Furthermore, the number of “ambiguous”examples suggests that the actual proportion of compound volcanic vents is likely to be larger than our conservative ~70% estimate.

It is possible we could have erroneously included a few impact craters, whose raised rim and ejecta are unclear or degraded, in the database as vent sites. If so, these would be in the “non-compound” category,

Table 1
Categorization of volcanic vent sites.

Category	All	All Image Percent	Confident Classification Percent	Good Images	Good Image Percent
Compound	131	42%	70%	77	71%
Not Compound	57	18%	30%	23	21%
Ambiguous	61	20%	–	9	8%
Unclassifiable	60	19%	–	–	–
Total	309	100%	100%	109	100%

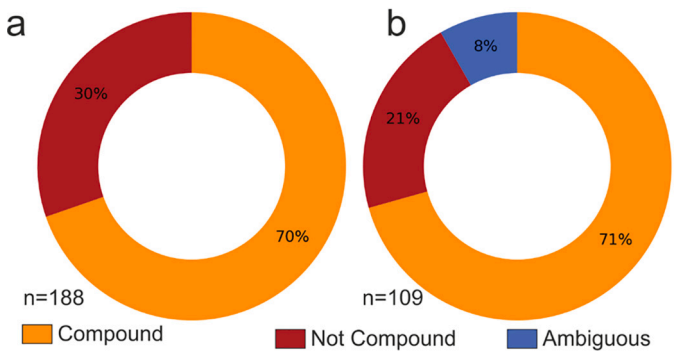

Fig. 4. doughnut charts of vent types on Mercury a. The ratio of compound to not-compound volcanic vents on Mercury from all resolvable vent sites in Table 1 (excluding those classified as 'ambiguous,' or 'unclassifiable'). b. The proportion of vent types in only those vent sites with best quality images (those vents listed as having 'good' image quality in Table 1).

because no common morphological feature of impact craters match those used to classify a vent site as compound. This would artificially reduce the proportion of compound volcanic vent sites, meaning that, if anything, compound vents are likely to be slightly more common than otherwise indicated.

For vents with no interior structures, and thus not considered compound, we should consider whether they are likely to have formed by repeated eruptions at the same spot. Candidates include vents whose brinks contain areas of both convex and concave planform shape. This could suggested shaping by mass wasting, but we observe that their floors often appear to lack mass wasting deposits such as positive relief features with lobate toes, so multiple eruptions are at least plausible here too. See the north of Fig. 3d for a rare example of an area where a slump is clearly observed, and so explains the planform of the vent wall in that area. In addition, any sites where later eruptions are larger than previous eruptions would likely not show signs of being compound.

We plot the geographical location of vents distinguished by type in Fig. 5. 79% of compound vents and 89% of non-compound vent sites are within impact craters or basins. These percentages are close to the ranges previously reported for all vents (of all types) within craters, such as 91% (Klimczak et al., 2018) or 81% (Thomas et al., 2014c).

3.1. Examples of compound vents

While assessing relative surface roughness within components of compound vents, we found no examples of conflicts between crosscutting relationships and relative age implied by surface roughness, as also identified within the vent in Agwo Facula (Rothery et al., 2014). To demonstrate variability in vent types and their morphology, and to investigate what this might tell us about explosive volcanism on Mercury, we discuss here four other examples of compound volcanic vent sites. These encompass the variety of form and illustrate some key features for deducing volcanic processes at such vents.

The first example is a large vent containing internal structures. The second is a smaller vent, but still with clear internal structures. The third focuses on small pits that we have identified within the very large Nathair Facula pit using high-resolution images, and that are not observed at other vent sites. The fourth is particularly unusual and is a dome that we identified within a vent, and which is a possible constructive feature.

Example 1. The vent site inside Kipling crater (Fig. 6). We used two images with opposite Sun azimuths to identify component vents. The overall compound volcanic vent is 15 km wide and 37 km long. We identified seven internal vents within it that demonstrate crosscutting relationships and textural variation, suggesting a complex eruptive history. Where possible, we used the crosscutting relationships of these depressions to infer a time sequence. The oldest element is probably the north of the complex (depression a). Depression *b* is deeper and truncates the southern end of a and so may be younger than depression a. Depression *c* cuts across depression *b* in a similar manner.

The area in the south of the vent (*f*/*g*) is the most texturally rough and cuts through the floor of *c* and *d*, so is probably more recently active. The youngest part, based on texture, is probably depression *g*. It is not possible to determine the age of *e* relative to the rest of the complex, because of an intervening septum in the form of a segmented ridge (that also divides depression *d* from *c*). The curved nature and position of this ridge within the lava-flooded floor of the host impact crater (Kipling) suggest that it may represent a remnant of Kipling's peak ring structure. It appears that there was a general progression of the locus of the eruption from north to south based on crosscutting relationships and textural roughness.

Example 2: 12 km × 13 km vent located in a plains-flooded re-entrant of the southern rim of the Caloris basin and within Ejo Faculae. This vent site provides another demonstration of internal crosscutting relationships (Fig. 7). We used image EN250796801M to map out depressions based on the crosscutting relationships of four or possibly five separate pits. Here, poorly-expressed depression *a* (little of which survives) is perhaps the oldest, though its brink is no longer clear. Depression *b* has the largest area. There may be additional vents within

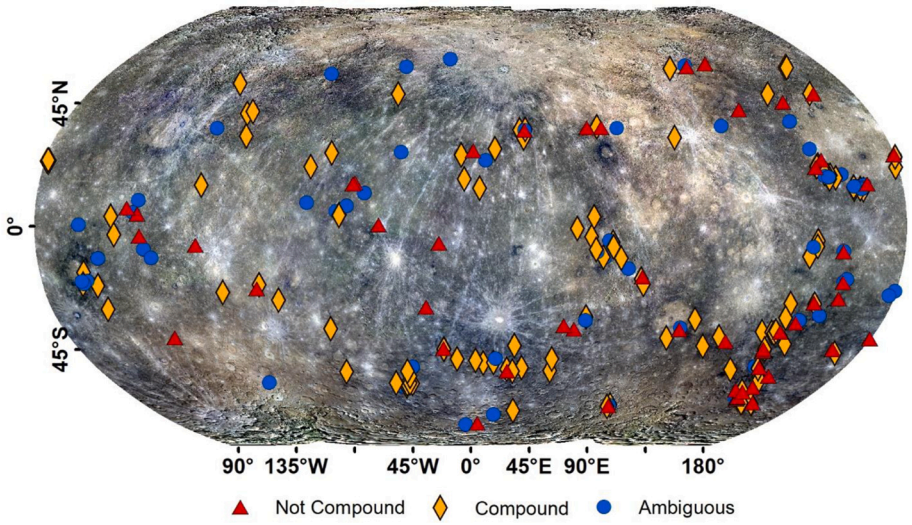

Fig. 5. Global distribution of vents in this study, superimposed on the global colour map (Denevi et al., 2016) using a Robinson projection.

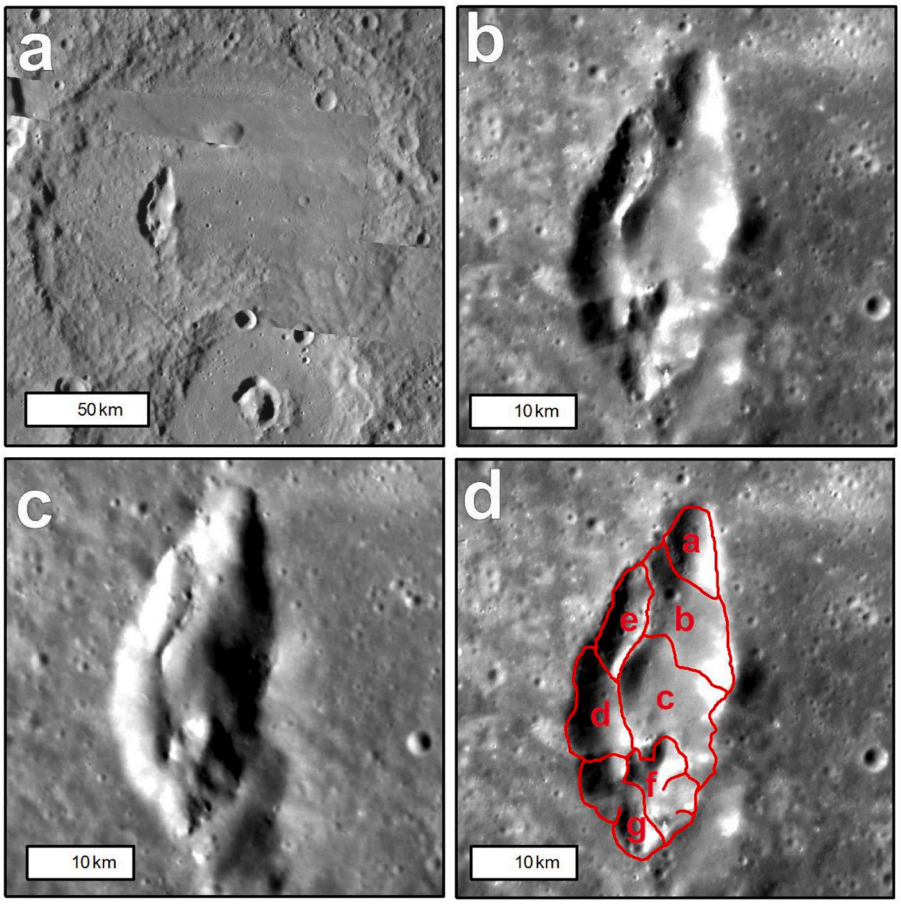

Fig. 6. A compound vent within Kipling crater. a. Overview of Kipling crater with the vent located in the crater floor, image centre 72°E 19°S, mosaic: (Denevi et al., 2018) b. Illumination from West EN0252180447M (69.7 m/ pixel). c. Image: EN1013780238M (156.8 m/ pixel) illumination from East d. EN0252180447M with interpreted vents (in approximate alphabetical order, oldest to youngest). Images b-d centred at 71.3°E, −19.2°N, North towards the top. Image credit: NASA/ Johns Hopkins University Applied Physics Laboratory/Carnegie Institution of Washington.

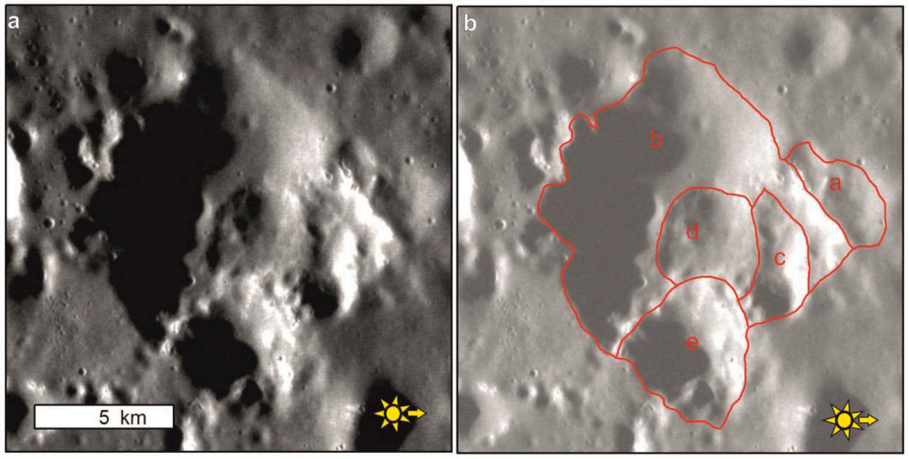

Fig. 7. A compound vent located in the south of the Caloris basin. a. Image centred at 159.3° E, 14.3° N using image EN250796801M (31.8 m/pixel). b. The same image with 40% transparency and interpreted vent history in alphabetical order according to relative age, oldest to youngest. North towards the top image, image credit: NASA/ Johns Hopkins University Applied Physics Laboratory/Carnegie Institution of Washington.

the shadowed area of *b*, but images with suitable illumination conditions are of insufficient resolution to confirm this. Depressions *c, d,* and *e* each cut into the floor of *b*. We interpret the divisions to represent a sequence of eruptions that occurred after *b*, with *e* probably being the most recent as it cuts across *c* and *d*, and a mantling deposit appears to overlie *b* and *d*.

Example 3. Nathair Facula is the largest facula on the planet and surrounds the largest (39 km × 30 km) recognised vent structure (Fig. 8). This vent is an unusual example. It lacks any distinct septa. However, the high resolution of available images (37.6 m/pixel) shows it to have multiple shallow bowl-like depressions in the floor that we interpret as separate eruption sites. The southern part of the vent floor has a smooth texture, the appearance of which is consistent with being an older area mantled by younger deposits. The floor in the northern half of the vent is rougher, and so is presumably not mantled and therefore likely to be younger. Within this northern section, much of the eastern

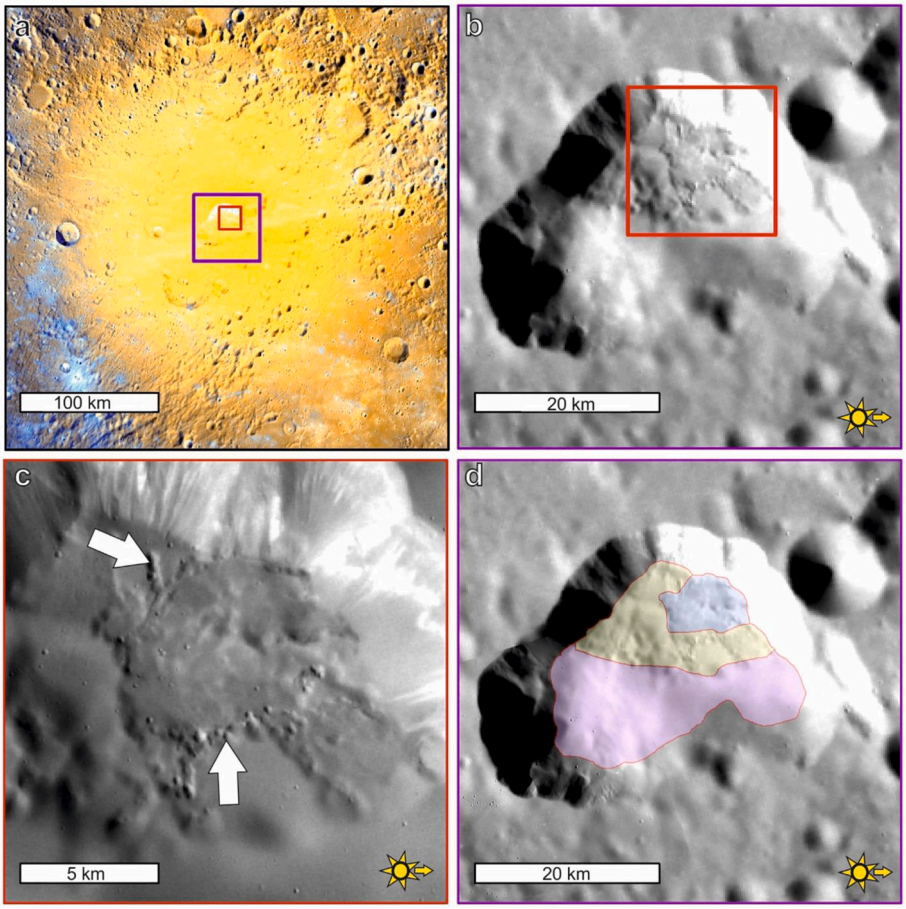

Fig. 8. The vent area inside Nathair Facula; north to the top in all images. a. Enhanced colour basemap (Denevi et al., 2016) showing Nathair Facula. Purple box shows the extent of b and d, and the red box the extent of c. b overview of the pit morphology. The rough texture is visible in the NE of the floor. Image: EW0254884916G (200 m/pixel). c: Arrows indicate examples of small pit features that outline the rougher area. Image EN0224508427 (37.6 m/ pixel). Both images are illuminated from the west. d. The floor of the pit divided into areas based on texture. EW0254884916G Image credit: NASA/ Johns Hopkins University Applied Physics Laboratory/Carnegie Institution of Washington. (For interpretation of the references to colour in this figure legend, the reader is referred to the web version of this article.)

part is rougher still, and thus likely the most recent site to have hosted significant eruptive activity (making up approximately 1/8th of the floor area of the vent). We have been conservative and classified it among the ambiguous compound vents in Table 1, although Rothery et al. (2021) give reasons for regarding it as compound. These include a stereo-derived digital elevation model (DEM) in Thomas et al. (2014c), which shows that the floor is deepest in the northern part of the vent, and suggests there were at least three eruptive sites within this vent (Fig. 8d).

Another remarkable feature within the vent at Nathair Facula is the presence of small pits on the floor. These pits are 100–600 m diameter, shallow, bowl-shaped depressions (Fig. 8c). They do not have the VIS-IR signature or high albedo that characterises hollows (Blewett et al., 2013; Chabot et al., 2011). They do not form the straight or arcuate chains typical of catenae (chains of secondary impact craters) and lack the raised rims associated with impact cratering. The pits are on a scale similar to some of the features seen in 'pitted ground'; however, no example of 'pitted ground' follows such a narrow pattern (Thomas et al., 2014c). These pits are on the boundary between a rough area of the floor and the smoother area surrounding it. If this area represents the most recent area of eruption, then these pits are on the edge of it possibly formed in the waning phases of an eruption. The small size of these pits means there is no clear way to date them; however, given the intensity of Nathair Facula (Besse et al., 2020; Rothery et al., 2021), parts of this vent may be relatively young compared to other vents on the planet. The pit's location outside a crater hampers dating, but Rothery et al. (2021) note that parts of the surrounding facula overlie ejecta from the c4 (Mansurian) crater Rachmaninoff, making the most recent eruption Mansurian or younger in age. If activity inside this compound vent is indeed atypically young, then comparable features in other vent sites may have been degraded beyond visibility by space weathering and impact gardening.

Example 4includes the only feature inside a vent that we regard as a plausible constructional feature. The pit is a 24 km × 15 km across clover leaf-shaped compound vent, containing a 500 m wide dome centred at 139.6°E, 48.5°N (Fig. 9) with hollows on its top. The dome's location on the floor of a vent demonstrates that it formed after the excavation of the vent. Unfortunately, the NW edge of the dome is shadowed, which could be hiding important morphological details. A positive topographic anomaly on the floor of a vent could have been produced by mass-wasting, but that is unlikely in this case as its top and edge on the side closest to the wall both appear to be convexly rounded (though the shadow impedes analysis). A more persuasive alternative is that it is a lava dome formed by very viscous lava, on a much smaller scale than the two possible constructional edifices identified by Wright et al. (2018). Better images and spectral data from the BepiColombo mission (Rothery et al., 2020) are likely to improve understanding of this unusual feature, including the fine scale texture on top of the dome, and we recommend it as a target for that mission.

3.2. *Asymmetric faculae*

Supporting evidence for vent migration comes from some of their surrounding faculae. Although the original appearance of a facula must depend on the strength and duration of the eruption, faculae are expected to fade as they age as a result of space weathering and impact gardening (e.g. Besse et al., 2020), resulting in the muting of their spectral signature and shrinkage of their visible extent. The unnamed facula inside Picasso crater (Fig. 10a,b) shows an uneven distribution along the length of the arcuate vent site. The facula is most intense

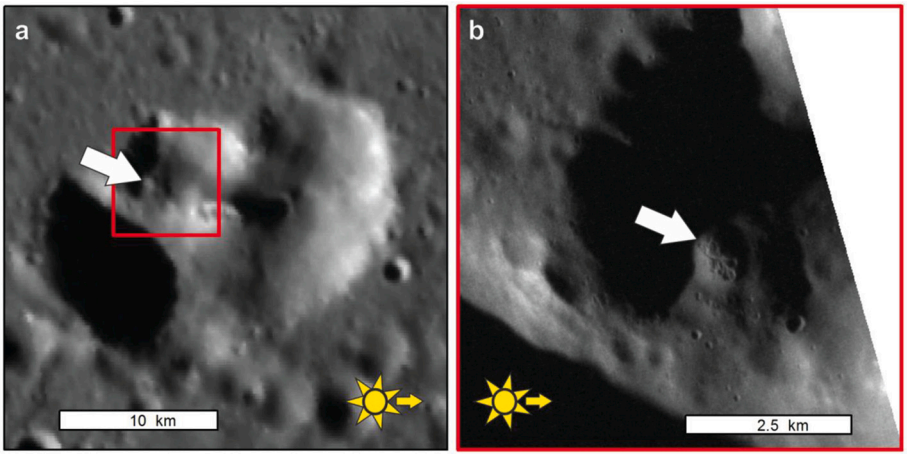

Fig. 9. A compound vent with a constructive feature a. Overview image from 166/m global basemap (Denevi et al., 2016) centred at 139.6°E, 48.5°N. North towards the top. This compound volcanic vent appears to comprise at least three separate smaller vents; the red box shows the location of b. b. Arrow points to the post-excavation structure within a vent that is a candidate for a post-eruptive edifice. Image EN0251055380M (13.5 m/pixel). Sun arrow shows illumination direction for clarity. Image credit: NASA/ Johns Hopkins University Applied Physics Laboratory/Carnegie Institution of Washington. (For interpretation of the references to colour in this figure legend, the reader is referred to the web version of this article.)

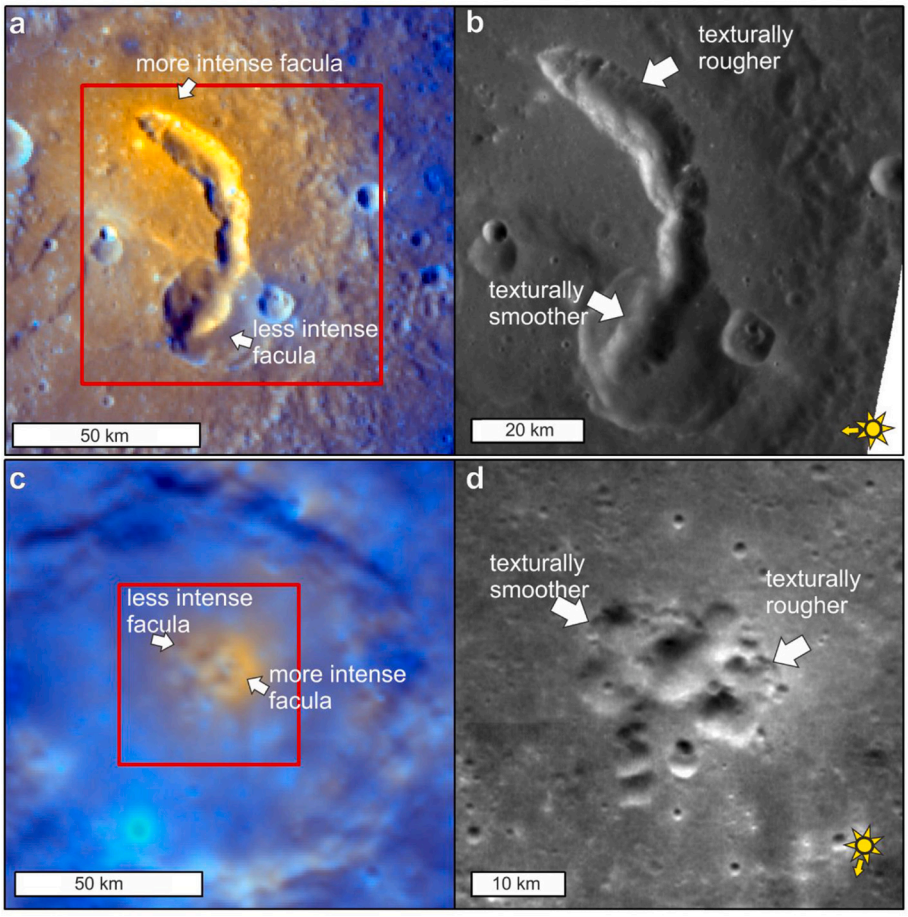

Fig. 10. Examples of asymmetric faculae a. Picasso crater showing the vent and facula in enhanced colour basemap (Denevi et al., 2018). The red box shows the location of b. b. Image EN0219816577M showing the compound vent inside Picasso crater (107 m/pixel). c. An unnamed facula within an unnamed impact crater; image centred at, −6.5° E – 48.4°N on enhanced colour basemap (Denevi et al., 2016). The red box shows compound vent sites in d. d. Detail of the compound vent sites inside the faculae seen in c. Image EN1034978249M (182 m / pixel). North towards the top of images. Image credit: NASA/ Johns Hopkins University Applied Physics Laboratory/Carnegie Institution of Washington. (For interpretation of the references to colour in this figure legend, the reader is referred to the web version of this article.)

around the north of the vent, correlating with the roughest textured area of vent floor and walls, which we would expect to indicate the most recent eruptions. The facula is weaker further south along the vent, and here the vent floor and walls show smoother textures suggesting that this area is older and was either mantled by later eruptions and then degraded, or just degraded by space weathering.

The second example of an asymmetric facula is seen associated with the compound vent in Fig. 10c,d, which is a cluster of vents around the centre of a complex crater whose floor was covered by a plains unit (likely to be lava) before being punctured by vents close to where the buried central peak (or peak complex) would be. The spectral anomaly is stronger near the east of this compound volcanic vent site, and the east of the vent site is texturally rougher than the west, suggesting it is younger and less degraded, which is consistent with the more intense area of facula being younger.

A third example is Nathair Facula (Fig. 8a), whose mid-point is displaced by between 10 and 30 km north or northeast relative to the centre of its vent complex as demonstrated by Rothery et al. (2020). This is consistent with the textural evidence in Fig. 8 that the youngest activity was in the north of the pit floor.

These asymmetric examples where facula intensity correlates with relative age as inferred age superpositional relationships and roughness

add corroborating evidence that some vents have undergone multiple eruptions, with the locus of activity migrating between eruption events. In the case of example 1 migration appears to have been from south to north along an arc tracing a probable buried a peak ring structure, in example 2 the roughness and facula asymmetry suggests the more recent activity was in the east of a cluster of vents. Better constraints on the rates at which faculae fade with age might improve constraints on when the activity occurred, especially in conjunction with spectral data to map out the extents of faculae (e.g., Besse et al., 2020).

4. Discussion

We now describe the general inferences and interpretations that follow from our overall compound vent statistics and from the evidence from individual examples that provide case studies of the processes that may have occurred more generally at volcanic vent sites. We then speculate on their implications (section 4.2).

4.1. General implications

The presence of such a high proportion of compound volcanic vents on Mercury suggests that more than a single event occurred at most vent sites, with migration of the locus of eruption in increments that can total up to about 50 km (for example, Fig. 10b). The question then arises as to whether these formed polygenetically (from multiple eruptions) or as part of a sequence within the same eruption (a monogenetic event).

The duration of any pause between eruptive episodes at successive vents within a compound vent site cannot be quantified directly. For example, vents have too small an area for valid crater statistics to be collected by measuring size-frequency distributions of superposed impact craters. Matters are made worse because secondary craters, which are typically clustered, may dominate the crater population up to 10 km crater diameter (Strom et al., 2011; Strom et al., 2008). Additionally, pyroclastic materials may not preserve impact craters in the same way as the surrounding regolith, hampering any comparisons between size-frequency distributions (Lucchitta and Schmitt, 1974). However, visibly apparent density differences of ~100 m diameter impact craters on the floors of individual depressions within compound volcanic vents at Agwo and Nathair Faculae (and perhaps in the vent in Kipling Crater; Fig. 6) correspond with the order of formation deduced from both crosscutting relationships and differences in surface roughness. We have found no counterexamples where the sequence of events deduced from cross-cutting relationships is contrary to the relative ages suggested by the density of small craters (fewer in younger component-vents) or textural roughness (rougher in younger components within a vent site). This supports the suggestion that significant time gaps occurred between the formation of the oldest and youngest component vents in at least some examples.

Examination of internal structure often reveals smaller vents cross-cutting, or entirely within, larger vents (e.g., Figs. 3c, 6, 7). This is consistent with the most recent eruptions having been less powerful and/or briefer than previous ones, as might be expected in a waning volcanic system. In the case of the vent in Nathair Facula, its last major eruption appears to occupy ~1/8th of the vent complex by area. We note that if the last eruption at any site was big enough this could result in a new pit large enough to destroy evidence of pre-existing smaller vents, whereas late-stage smaller vents can crosscut, but not obliterate, pre-existing larger vents. However the lack of numerous large non-compound vents surrounded by prominent faculae suggest that this rarely happens, and that waning eruption size is indeed the norm.

The putative lava dome seen in Example 4 (Fig. 9), and the small pits at the edge of the youngest vent site within Nathair Facula (Fig. 8c), both suggest later phases of less intense activity at these vent sites, and a terminal switch from explosive to effusive volcanism in the former example.

The composition of faculae around vents is not necessarily the same in every case (Besse et al., 2020). Furthermore, spatial variations of the intensities of faculae around vent sites (Section 3.2) indicate that eruption strength and/or duration varied within vent sites, or that some faculae are sufficiently older than others to exhibit different degrees of muting by space weathering and mixing into the background by impact gardening. These factors are consistent with vents having undergone multiple eruptions. A detailed study examining the distribution of faculae around vents in terms of composition and thickness may help to refine the eruption history of compound volcanic vents.

4.2. How did the eruptions occur?

Possible mechanisms for the formation of these vents are explosive excavation, collapse into an evacuated conduit, such as a dyke, or a combination of these (Jozwiak et al., 2018). We concur with Rothery et al. (2014) in observing no surface features indicative of ring faults, as usually associated with terrestrial and Martian caldera collapse, though they cannot be excluded.

Some terrestrial examples of phreatomagmatic and kimberlite eruptions can undergo migration of the diatreme during a single eruption. Being a continual migration process, such migration is unlikely to leave septa dividing the vent (White and Ross, 2011), but this could be analogous to the process on Mercury resulting in vents with a sinuous brink but no internal features (which we classed as not compound vents). Multiple separate eruptions using the same conduit with pauses could, however, lead to multiple component vents at a locality (Fulop and Kurszlaukis, 2017) manifested at compound vent sites as discrete vents or vents divided by septa.

If compound vents form as collapse pits above a dyke, collapse occurs into the dyke that had fed them (Wilson et al., 2011; Wilson and Head, 2017). A flat, rather than bowl-shaped, floor is expected, as found within lunar rilles (Wilson et al., 2011), although a deeper top to the dyke could enable bowl-shaped pits to form without a continuous rille (Jozwiak et al., 2018). This would suggest that each component vent was formed sequentially as part of the same eruption. This may match with sequential vent sites in the style of the example within Picasso crater. At the vent site within Nathair Facula, dykes might explain the formation of the small young pits on the vent floor (Fig. 8c).

Given individual vents' bowl-like profiles suggested by photogeology (e.g. Figs. 7, 9), LIDAR tracks (Thomas et al., 2014a) and digital elevation model data (e.g. the 'simple vents' in Jozwiak et al. (2018) and Thomas et al. (2014a)), we favour excavation by explosive eruption as the main pit-forming process. However, we note that it seems inevitable that after termination of eruption various collapse processes would have choked the evacuated conduit and modified the surrounding pit walls. It is probable that both explosive excavation and collapse is needed on Mercury to explain the variety of features seen.

Regardless of formation mechanism, the asymmetry of the facula at Picasso, and the progression in eruption identified in the vent site at Agwo Facula (Rothery et al., 2014) and in example 2 (Fig. 10c,d) suggests that at some compound vent sites there were pauses between the formation of individual component vents. To enable this, a mechanism is needed to recharge the volatiles. It also suggests that local stress regimes were conducive to eruptions over a potentially extended period of time.

4.3. Volatile recharge

For multiple explosive eruptions to occur, each eruption must be followed by recharge of volatiles capable of exsolving as the gases needed to drive the next eruption. Such recharge could take place by: (i) recharge in the source (mantle volatiles), (ii) recharge within the melt (for example, by assimilation or fractionation), or (iii) processes within the feeder dyke (Head and Wilson, 2017).

On Mercury, the volatile component of the melt is most likely to be dominated by CO and SO_2 (Kerber et al., 2009; Weider et al., 2016). The only pyroclastic deposit large enough to have had its composition

measured by MESSENGER is Nathair Facula (Peplowski et al., 2016; Weider et al., 2016), which is relatively depleted in both sulfur and carbon. This is consistent with iron silicates in the magma having been reduced by the carbon (McCubbin et al., 2017) and sulfur to generate the gases needed for explosivity, so that sulfur and carbon are therefore mostly absent from the solid pyroclastic ejecta.

Mercury's crust is rich in volatile elements with up to 4 wt% sulfur (Nittler et al., 2011). The low reflectance material (LRM), which is probably derived from the lower crust, may be enriched in other volatiles including up to 5 wt% carbon (Klima et al., 2018; Murchie et al., 2015; Peplowski et al., 2016). The LRM may now be present as horizons at several depths in Mercury's crust, occurring as ejecta layers redistributed from a graphite-rich primary crust or buried ancient lava flows (Klima et al., 2018; Peplowski et al., 2016; Vander Kaaden and McCubbin, 2015). The subsurface lateral continuity of the LRM source has yet to be constrained, but LRM may constitute a widespread source of volatiles that could be assimilated by melts during ascent.

Assimilation of stratigraphically controlled volatiles (i.e., in layers) into a dyke is likely to be inefficient due to the relatively small surface area of a dyke in contact with any horizon in the crust. A sill morphology would be more effective at assimilating volatiles because sills have significantly more surface area that could be in contact with a horizontal or sub-horizontal volatile-rich layer. If volatiles were assimilated multiple times from the same place in the crust, then this might require either stoping (collapse of the ceiling above a sill or larger intrusion) or migration of volatiles through the crust to replenish the volatiles before each episode of assimilation. Sills are more likely to form in a global contractional environment than dykes (e.g. Byrne et al., 2018; Watanabe et al., 1999). Current remote sensing data for Mercury provide insufficient evidence to be able to identify whether a sill or dyke morphology is more common, although the lack of observed floor deformation (specifically fracturing) in craters that have explosive vents on their floors makes shallow sills unlikely, and so favours dykes or deep sills (Jozwiak et al., 2018; Thomas et al., 2015).

A second explanation for volatile availability may be that the partial melting zones in Mercury's mantle are rich in volatiles (Vander Kaaden and McCubbin, 2015). Direct connections between the mantle and the surface would allow volatile-rich melts within the mantle to ascend and resupply volcanic vents with new ('juvenile') volatiles.

It is often stated that Mercury's contractional tectonic regime is not conducive to magma ascent (Byrne et al., 2016; Michel et al., 2013; Tosi et al., 2013). This may explain why there are only about 300 identified explosive vent sites on the entire planet. Repeated eruptions at individual sites imply long-term connectivity to the melt source. The local stress regime must allow repeated magma ascent for eruptions to recur at dykes at these sites. It is not surprising, therefore, that the majority of volcanic vents occur within impact craters, because the crust below crater floors is expected to be highly fractured (Klimczak et al., 2018), or near thrust faults where localised stress changes could dilate certain fracture sets (Habermann and Klimczak, 2015). However, this does not explain all the identified vents: the vent inside Nathair Facula is neither inside an impact structure, nor close to a lobate scarp, for example, so other causes of localised differences in lithospheric stresses may be at play, such as variable crustal composition which can lead to local differences in strain (Galluzzi et al., 2019).

A third mechanism for volatile recharge is melt overturn within a dyke, in which volatile-rich magma is brought up from deeper in the dyke to replace an upper zone that had been passively or eruptively degassed (Head and Wilson, 2017). Additionally, if there is a main dyke at depth when the critical pressure builds up, it may spawn smaller dykes which would lead to smaller local eruptions within a system (Jozwiak et al., 2018). As the magma is stored in the dyke, and so does not need local stress regime differences to operate, no further connection with melt sources is required. This mechanism would allow only short intervals between eruptive events before the magma solidified, and so could not account for the contrasting ages suggested by small scale cratering seen inside the Agwo Facula compound vent (Rothery et al., 2014), unless associated with a deeper feeder dyke with smaller individual offshoots each producing an individual vent site.

Bearing in mind Mercury's contractional tectonic regime and accepting the tentative evidence for prolonged pauses between eruptions at each site, we suggest that the existence of polygenetic vents implies that long-lasting local stress anomalies, for example close to thrust faults (Habermann and Klimczak, 2015), must have been present to allow continued melt supply from the mantle in at least some examples.

5. Conclusions

Where image data have adequate resolution and quality, at least ~70% of volcanic vent sites on Mercury are compound, reflecting multiple eruption loci and potentially a polygenetic history. Many of the large vents that we do not classify as compound may have lost their internal structures over time and so could also be polygenetic, or could have formed by migration of the locus of an eruption in a fashion insufficiently punctuated to leave intervening septa.

At compound vents and other polygenetic sites, the volatiles within the erupting magma, necessary for an explosive eruption, were recharged, either at the melt source, in the crust, or by some process within magma stored in the crust. Volatile recharge has implications for the internal plumbing of these sites, suggesting that, once established, eruption sites can undergo multiple events occurring over a prolonged but currently weakly constrained duration. If additional volatile supply was from mantle sources, then the local stress regimes must have allowed repeated connection between source and vent. Otherwise, volatiles must have been assimilated from the crust, which probably requires recharge by movement of volatiles through the crust.

Migration of the locus of eruption must be considered when studying the extent of the explosive ejecta deposits that constitute faculae. A single central vent source is often modelled (Brož et al., 2018; Kerber et al., 2009), but the dynamic histories shown by our examples suggest that these sites relocate over time. Build-up of faculae from multiple eruption loci could extend the area covered by faculae without needing stronger eruptions, meaning that models using single source point estimates would over-estimate the eruptive power. These vents and their faculae should be high priorities for study by BepiColombo.

Data availability

The image data products used in this paper are publicly available from the Planetary Data System (PDS). The table of images can be found at https://ordo.open.ac.uk/articles/dataset/List_of_images_and_vent_ID_s_used_to_classify_vents/12058233 The list of vents at https://ordo.open.ac.uk/articles/dataset/Locations_and_Classifications_of_Vents_on_Mercury/12033876 MESSENGER data credited to NASA/Johns Hopkins University Applied Physics Laboratory/Carnegie Institute of Washington.

Declaration of Competing Interest

None.

Acknowledgments

Thanks to Ben Man, who found some additional vent locations. David Pegg was funded by the UK Science and Technology Facilities Council (STFC) under grant ST/R504993/1. DAR and MJB receive support from European Commission Grant 776276 (Planmap) for Mercury mapping. SJC is grateful for financial support from the French Space Agency CNES for her BepiColombo work. The authors declare no conflicts of interest. Thank you to Christian Klimczak and one anonymous reviewer for your help in making this a better paper.

References

Allum, J.A.E., 2013. Photogeology and Regional Mapping. Elsevier.

Banks, M.E., Xiao, Z., Braden, S.E., Marchi, S., Chapman, C.R., Barlow, N.G., Fassett, C.I., 2016. Revised age constraints for Mercury's Kuiperian and Mansurian systems. In: 47th Lunar Planet. Sci. Conf. Abstract 2943. https://doi.org/10.1016/j.icarus.2007.12.027.

Besse, S., Doressoundiram, A., Barraud, O., Griton, L., Cornet, T., Muñoz, C., Varatharajan, I., Helbert, J., 2020. Spectral properties and physical extent of pyroclastic deposits on mercury: variability within selected deposits and implications for explosive volcanism. J. Geophys. Res. Planets 125, 1–13. https://doi.org/10.1029/2018je005879.

Blewett, D.T., Chabot, N.L., Denevi, B.W., Ernst, C.M., Head, J.W., Izenberg, N.R., Murchie, S.L., Solomon, S.C., Nittler, L.R., McCoy, T.J., Xiao, Z., Baker, D.M.H., Fassett, C.I., Braden, S.E., Oberst, J., Scholten, F., Preusker, F., Hurwitz, D.M., 2011. Hollows on Mercury: MESSENGER evidence for geologically recent volatile-related activity. Science (80-.) 333, 1856–1859. https://doi.org/10.1126/science.1211681.

Blewett, D.T., Vaughan, W.M., Xiao, Z., Chabot, N.L., Denevi, B.W., Ernst, C.M., Helbert, J., D'Amore, M., Maturilli, A., Head, J.W., Solomon, S.C., 2013. Mercury's hollows: constraints on formation and composition from analysis of geological setting and spectral reflectance. J. Geophys. Res. E Planets 118, 1013–1032. https://doi.org/10.1029/2012JE004174.

Broxton, M.J., Edwards, L.J., 2008. The Ames Stereo Pipeline: automated 3D surface reconstruction from orbital imagery. In: Lunar and Planetary Science Conference, 39 (#2419).

Brož, P., Čadek, O., Wright, J., Rothery, D.A., 2018. The apparent absence of kilometer-sized pyroclastic volcanoes on mercury: are we looking right? Geophys. Res. Lett. 45, 12,171–12,179. https://doi.org/10.1029/2018GL079902.

Brunetti, M.T., Xiao, Z., Komatsu, G., Peruccacci, S., Guzzetti, F., 2015. Large rock slides in impact craters on the moon and mercury. Icarus 260, 289–300. https://doi.org/10.1016/j.icarus.2015.07.014.

Byrne, P.K., Ostrach, L.R., Fassett, C.I., Chapman, C.R., Denevi, B.W., Evans, A.J., Klimczak, C., Banks, M.E., Head, J.W., Solomon, S.C., 2016. Widespread effusive volcanism on mercury likely ended by about 3.5 Ga. Geophys. Res. Lett. 43, 7408–7416. https://doi.org/10.1002/2016GL069412.

Byrne, P.K., Whitten, J.L., Klimczak, C., McCubbin, F.M., Ostrach, L.R., 2018. The volcanic character of mercury. In: Mercury: The View after MESSENGER. Cambridge University Press, Cambridge, pp. 287–323.

Chabot, N.L., Denevi, B.W., Solomon, S.C., Xiao, Z., Ernst, C.M., Oberst, J., Blewett, D.T., Nittler, L.R., Preusker, F., Braden, S.E., Murchie, S.L., Head, J.W., Fassett, C.I., McCoy, T.J., Scholten, F., Hurwitz, D.M., Baker, D.M.H., Izenberg, N.R., 2011. Hollows on Mercury: MESSENGER evidence for geologically recent volatile-related activity. Science (80-.) 333, 1856–1859. https://doi.org/10.1126/science.1211681.

Davidson, J., De Silva, S., 2000. Composite volcanoes. In: Encyclopeida of Volcanoes, 1, pp. 663–681.

Denevi, B.W., Seelos, F.P., Ernst, C.M., Keller, M.R., Chabot, N.L., Murchie, S.L., Domingue, D.L., Hash, C.D., Blewett, D.T., 2016. Final calibration and multispectral map products from the mercury dual imaging system wide-angle camera. In: Lunar and Planetary Science Conference, p. 1264.

Denevi, B.W., Chabot, N.L., Murchie, S.L., Becker, K.J., Blewett, D.T., Domingue, D.L., Ernst, C.M., Hash, C.D., Hawkins, S.E., Keller, M.R., Laslo, N.R., Nair, H., Robinson, M.S., Seelos, F.P., Stephens, G.K., Turner, F.S., Solomon, S.C., 2018. Calibration, projection, and final image products of MESSENGER's mercury dual imaging system. Space Sci. Rev. 214, 2. https://doi.org/10.1007/s11214-017-0440-y.

Fulop, A., Kurszlaukis, S., 2017. Monogenetic v. polygenetic kimberlite volcanism: in-depth examination of the tango extension super structure, Attawapiskat kimberlite field, Ontario, Canada. Geol. Soc. Spec. Publ. 446, 205–224. https://doi.org/10.1144/SP446.7.

Galluzzi, V., Ferranti, L., Massironi, M., Giacomini, L., Guzzetta, L., Palumbo, P., 2019. Structural analysis of the Victoria quadrangle fault systems on mercury: timing, geometries, kinematics and relationship with the high-mg region. J. Geophys. Res. https://doi.org/10.1029/2019je005953.

Goudge, T.A., Head, J.W., Kerber, L., Blewett, D.T., Denevi, B.W., Domingue, D.L., Gillis-Davis, J.J., Gwinner, K., Helbert, J., Holsclaw, G.M., Izenberg, N.R., Klima, R.L., McClintock, W.E., Murchie, S.L., Neumann, G.A., Smith, D.E., Strom, R.G., Xiao, Z., Zuber, M.T., Solomon, S.C., 2014. Global inventory and characterisation of pyroclastic deposits on mercury: new insights into pyroclastic activity from MESSENGER orbital data. J. Geophys. Res. Planets 119, 635–658. https://doi.org/10.1002/2013JE004480.

Greeley, R., Spudis, P.D., 1981. Volcanism on mars. Rev. Geophys. Sp. Phys. 19, 13–41.

Habermann, M., Klimczak, C., 2015. Tectonic controls on pyroclastic volcanism on Mercury. In: AGU Fall Meeting Abstracts, pp. P53A–2101.

Hawkins, S.E., Boldt, J.D., Darlington, E.H., Espiritu, R., Gold, R.E., Gotwols, B., Grey, M.P., Hash, C.D., Hayes, J.R., Jaskulek, S.E., Kardian, C.J., Keller, M.R., Malaret, E.R., Murchie, S.L., Murphy, P.K., Peacock, K., Prockter, L.M., Reiter, R.A., Robinson, M.S., Schaefer, E.D., Shelton, R.G., Sterner, R.E., Taylor, H.W., Watters, T.R., Williams, B.D., 2007. The mercury dual imaging system on the MESSENGER spacecraft. Space Sci. Rev. 131, 247–338. https://doi.org/10.1007/s11214-007-9266-3.

Head, J.W., Wilson, L., 2017. Generation, ascent and eruption of magma on the moon: new insights into source depths, magma supply, intrusions and effusive/explosive eruptions (part 2: predicted emplacement processes and observations). Icarus 283, 176–223. https://doi.org/10.1016/j.icarus.2016.05.031.

Head, J.W., Murchie, S.L., Prockter, L.M., Solomon, S.C., Chapman, C.R., Strom, R.G., Watters, T.R., Blewett, D.T., Gillis-Davis, J.J., Fassett, C.I., Dickson, J.L., Morgan, G. A., Kerber, L., 2009. Volcanism on mercury: evidence from the first MESSENGER flyby for extrusive and explosive activity and the volcanic origin of plains. Earth Planet. Sci. Lett. 285, 227–242. https://doi.org/10.1016/j.epsl.2009.03.007.

Jackson, J.A., Bates, R.L., 1997. Glossary of Geology (American Geological Institute).

Jozwiak, L.M., Head, J.W., Wilson, L., 2018. Explosive volcanism on mercury: analysis of vent and deposit morphology and modes of eruption. Icarus 302, 191–212. https://doi.org/10.1016/j.icarus.2017.11.011.

Kerber, L., Head, J.W., Solomon, S.C., Murchie, S.L., Blewett, D.T., Wilson, L., 2009. Explosive volcanic eruptions on mercury: eruption conditions, magma volatile content, and implications for interior volatile abundances. Earth Planet. Sci. Lett. 285, 263–271. https://doi.org/10.1016/j.epsl.2009.04.037.

Kerber, L., Head, J.W., Blewett, D.T., Solomon, S.C., Wilson, L., Murchie, S.L., Robinson, M.S., Denevi, B.W., Domingue, D.L., 2011. The global distribution of pyroclastic deposits on mercury: the view from MESSENGER flybys 13. Planet. Space Sci. 59, 1895–1909. https://doi.org/10.1016/j.pss.2011.03.020.

Klemetti, E.W., Grunder, A.L., 2008. Volcanic evolution of Volcán Aucanquilcha: a long-lived dacite volcano in the Central Andes of northern Chile. Bull. Volcanol. 70, 633–650. https://doi.org/10.1007/s00445-007-0158-x.

Klima, R.L., Denevi, B.W., Ernst, C.M., Murchie, S.L., Peplowski, P.N., 2018. Global distribution and spectral properties of low-reflectance material on mercury. Geophys. Res. Lett. 45, 2945–2953. https://doi.org/10.1002/2018GL077544.

Klimczak, C., Byrne, P.K., Solomon, S.C., 2015. A rock-mechanical assessment of Mercury's global tectonic fabric. Earth Planet. Sci. Lett. 416, 82–90. https://doi.org/10.1016/j.epsl.2015.02.003.

Klimczak, C., Crane, K.T., Habermann, M.A., Byrne, P.K., 2018. The spatial distribution of Mercury's pyroclastic activity and the relation to lithospheric weaknesses. Icarus 315, 115–123. https://doi.org/10.1016/j.icarus.2018.06.020.

Lucchitta, B.K., Schmitt, H.H., 1974. Orange material in the Sulpicius Gallus formation at the southwestern edge of Mare Serenitatis. Proc. Fifth Lunar Conf. 1, 223–234.

Lyell, C., 1853. Principles of Geology, 9th ed. Spottswoodes and Shaw, London.

Malliband, C.C., Conway, S.J., Rothery, D.A., Balme, M.R., 2019. Potential identification of downslope mass movements on mercury driven by volatile-loss. In: Lunar and Planetary Science Conference 2019, p. 1804.

McCubbin, F.M., Vander Kaaden, K.E., Peplowski, P.N., Bell, A.S., Nittler, L.R., Boyce, J.W., Evans, L.G., Keller, L.P., Elardo, S.M., McCoy, T.J., 2017. A low O/Si ratio on the surface of mercury: evidence for silicon smelting? J. Geophys. Res. Planets 122, 2053–2076. https://doi.org/10.1002/2017JE005367.

Michel, N.C., Hauck, S.A., Solomon, S.C., Phillips, R.J., Roberts, J.H., Zuber, M.T., 2013. Thermal evolution of mercury as constrained by MESSENGER observations. J. Geophys. Res. E Planets 118, 1033–1044. https://doi.org/10.1002/jgre.20049.

Murchie, S.L., Klima, R.L., Denevi, B.W., Ernst, C.M., Keller, M.R., Domingue, D.L., Blewett, D.T., Chabot, N.L., Hash, C.D., Malaret, E., Izenberg, N.R., Vilas, F., Nittler, L.R., Gillis-Davis, J.J., Head, J.W., Solomon, S.C., 2015. Orbital multispectral mapping of mercury with the MESSENGER mercury dual imaging system: evidence for the origins of plains units and low-reflectance material. Icarus 254, 287–305. https://doi.org/10.1016/j.icarus.2015.03.027.

Neuendorf, K.K.E., Mehl, J.P., Jackson, J.A., 2005. Glossary of Geology, 5th ed. American Geological Institute, Alexandria, Va.

Nittler, L.R., Starr, R.D., Weider, S.Z., McCoy, T.J., Boynton, W.V., Ebel, D.S., Ernst, C.M., Evans, L.G., Goldsten, J.O., Hamara, D.K., Lawrence, D.J., McNutt, R.L., Schlemm, C.E., Solomon, S.C., Sprague, A.L., 2011. The major-element composition of Mercury's surface from MESSENGER X-ray spectrometry. Science (80-.) 333, 1847–1850. https://doi.org/10.1126/science.1211567.

Peplowski, P.N., Klima, R.L., Lawrence, D.J., Ernst, C.M., Denevi, B.W., Frank, E.A., Goldsten, J.O., Murchie, S.L., Nittler, L.R., Solomon, S.C., 2016. Remote sensing evidence for an ancient carbon-bearing crust on mercury. Nat. Geosci. 9, 273–276. https://doi.org/10.1038/ngeo2669.

Rava, B., Hapke, B., 1987. An analysis of the mariner 10 color ratio map of mercury. Icarus 71, 397–429. https://doi.org/10.1016/0019-1035(87)90037-6.

Rothery, D.A., Thomas, R.J., Kerber, L., 2014. Prolonged eruptive history of a compound volcano on mercury: volcanic and tectonic implications. Earth Planet. Sci. Lett. 385, 59–67. https://doi.org/10.1016/j.epsl.2013.10.023.

Rothery A, David, Barraud, Océane, Besse, Sebastien, Carli, Cristian, Pegg L, David, Wright, Jack, 2021. On the asymmetry of Nathair Facula, Mercury. Icarus 355, 114180. https://doi.org/10.1016/j.icarus.2020.114180.

Rothery, D.A., Massironi, M., Alemanno, G., Barraud, O., Besse, S., Bott, N., Brunetto, R., Bunce, E., Byrne, P., Capaccioni, F., Capria, M.T., Carli, C., Charlier, B., Cornet, T., Cremonese, G., D'Amore, M., De Sanctis, M.C., Doressoundiram, A., Ferranti, L., Filacchione, G., Galluzzi, V., Giacomini, L., Grande, M., Guzzetta, L.G., Helbert, J., Heyner, D., Hiesinger, H., Hussmann, H., Hyodo, R., Kohout, T., Kozyrev, A., Litvak, M., Lucchetti, A., Malakhov, A., Malliband, C., Mancinelli, P., Martikainen, J., Martindale, A., Maturilli, A., Milillo, A., Mitrofanov, I., Mokrousov, M., Morlok, A., Muinonen, K., Namur, O., Owens, A., Nittler, L.R., Oliveira, J.S., Palumbo, P., Pajola, M., Pegg, D.L., Penttilä, A., Politi, R., Quarati, F., Re, C., Sanin, A., Schulz, R., Stangarone, C., Stojic, A., Tretiyakov, V., Väisänen, T., Varatharajan, I., Weber, I., Wright, J., Wurz, P., Zambon, F., 2020. Rationale for BepiColombo studies of Mercury's surface and composition. Space Sci. Rev. 216, 66. https://doi.org/10.1007/s11214-020-00694-7.

Strom, R.G., Chapman, C.R., Merline, W.J., Solomon, S.C., Head, J.W., 2008. Mercury cratering record viewed from MESSENGER's first flyby. Science (80-.) 321, 79–81. https://doi.org/10.1126/science.1159317.

Strom, R.G., Banks, M.E., Chapman, C.R., Fassett, C.I., Forde, J.A., Head, J.W., Merline, W.J., Prockter, L.M., Solomon, S.C., 2011. Mercury crater statistics from MESSENGER flybys: implications for stratigraphy and resurfacing history. Planet. Space Sci. 59, 1960–1967. https://doi.org/10.1016/j.pss.2011.03.018.

Thomas, R.J., Rothery, D.A., Conway, S.J., Anand, M., 2014a. Mechanisms of explosive volcanism on mercury: implications from its global distribution and morphology. J. Geophys. Res. E Planets 119, 2239–2254. https://doi.org/10.1002/2014JE004692.

Thomas, R.J., Rothery, D.A., Conway, S.J., Anand, M., 2014b. Long-lived explosive volcanism on mercury. Geophys. Res. Lett. 41, 6084–6092. https://doi.org/10.1002/2014GL061224.

Thomas, R.J., Rothery, D.A., Conway, S.J., Anand, M., 2014c. Hollows on mercury: materials and mechanisms involved in their formation. Icarus 229, 221–235. https://doi.org/10.1016/j.icarus.2013.11.018.

Thomas, R.J., Rothery, D.A., Conway, S.J., Anand, M., 2015. Explosive volcanism in complex impact craters on mercury and the moon: influence of tectonic regime on depth of magmatic intrusion. Earth Planet. Sci. Lett. 431, 164–172. https://doi.org/10.1016/j.epsl.2015.09.029.

Tosi, N., Grott, M., Plesa, A.C., Breuer, D., 2013. Thermochemical evolution of Mercury's interior. J. Geophys. Res. E Planets 118, 2474–2487. https://doi.org/10.1002/jgre.20168.

Vander Kaaden, K.E., McCubbin, F.M., 2015. Exotic crust formation on mercury: consequences of a shallow, FeO-poor mantle. J. Geophys. Res. Planets 120, 195–209. https://doi.org/10.1002/2014JE004733.

Watanabe, T., Koyaguchi, T., Seno, T., 1999. Tectonic stress controls on ascent and emplacement of magmas. J. Volcanol. Geotherm. Res. 91, 65–78. https://doi.org/10.1016/S0377-0273(99)00054-2.

Weider, S.Z., Nittler, L.R., Murchie, S.L., Peplowski, P.N., McCoy, T.J., Kerber, L., Klimczak, C., Ernst, C.M., Goudge, T.A., Starr, R.D., Izenberg, N.R., Klima, R.L., Solomon, S.C., 2016. Evidence from MESSENGER for sulfur- and carbon-driven explosive volcanism on mercury. Geophys. Res. Lett. 43, 3653–3661. https://doi.org/10.1002/2016GL068325.

White, J.D.L., Ross, P., 2011. Maar-diatreme volcanoes : A review. J. Volcanol. Geotherm. Res. 201, 1–29. https://doi.org/10.1016/j.jvolgeores.2011.01.010.

Wilson, L., 2009. Volcanism in the solar system. Nat. Publ. Gr. 2, 389–397. https://doi.org/10.1038/ngeo529.

Wilson, L., Head, J.W., 1983. A comparison of volcanic eruption processes on Earth, Moon, Mars, Io and Venus. Nature 302, 663–669. https://doi.org/10.1038/302663a0.

Wilson, L., Head, J.W., 2017. Generation, ascent and eruption of magma on the Moon: new insights into source depths, magma supply, intrusions and effusive/explosive eruptions (part 2: theory). Icarus 283, 146–175. https://doi.org/10.1016/j.icarus.2015.12.039.

Wilson, L., Hawke, B.R., Giguere, T.A., Petrycki, E.R., 2011. An igneous origin for Rima Hyginus and Hyginus crater on the Moon. Icarus 215, 584–595. https://doi.org/10.1016/j.icarus.2011.07.003.

Wood, C.A., Radebaugh, J., 2020. Morphologic Evidence for Volcanic Craters near Titan ' S North Polar Region, pp. 0–3. https://doi.org/10.1029/2019JE006036.

Wright, J., Rothery, D.A., Balme, M.R., Conway, S.J., 2018. Constructional Volcanic Edifices on Mercury: Candidates and Hypotheses of Formation, pp. 1–20. https://doi.org/10.1002/2017JE005450.